J|A|C|S
ARTICLES
Published on Web 03/06/2002

Formation of Cyclodimeric (sp^2-C_1)-Bridged Cp/-Oxido ("CpC_1O"$M^{IV}X_2$) Group 4 Metal Ziegler−Natta Catalyst Systems—How Important Is the "Constrained Geometry" Effect?

Klaus Kunz,[†] Gerhard Erker,*[,†] Gerald Kehr,[†] Roland Fröhlich,[†,‡] Heiko Jacobsen,[§] Heinz Berke,[§] and Olivier Blacque[§]

Contribution from the Organisch-Chemisches Institut der Universität Münster, Corrensstrasse 40, D-48149 Münster, Germany, and Anorganisch-Chemisches Institut der Universität Zürich, Winterthurerstrasse 190, CH-8057 Zürich, Switzerland

Received April 12, 2001

Abstract: Deprotonation of sodium acetylcyclopentadienide (**11**) was achieved by treatment with LDA in THF to generate the dianion equivalent [Cp−C(=CH_2)−O]$^{2-}$ (**12**). Transmetalation with $Cl_2Ti(NMe_2)_2$ gave {[Cp−C(=CH_2)−O]Ti(NMe_2)$_2$}$_2$ (**17**); treatment of **12** with $Cl_2Zr(NEt_2)_2(THF)_2$ furnished {[Cp−C(=CH_2)−O]-Zr(NEt_2)$_2$}$_2$ (**18**). Cryoscopy in benzene revealed a dimeric structure of **18** in solution. Complex **18** was characterized further by an X-ray crystal structure analysis and by DFT calculations. The two zirconium centers of **18** are connected by means of two symmetry-equivalent η^5:κO[Cp−C(=CH_2)−O] ligands. The ligand backbone shows no specific steric constraints, different from the formally related "constrained geometry" systems such as [Cp*−$SiMe_2$−$NCMe_3$]Zr(NMe_2)$_2$ (**1b**). Nevertheless, upon treatment with MAO the CpCO group 4 metal complex system (**18**) generates an active homogeneous Ziegler−Natta catalyst for effective ethene/1-octene copolymerization, with up to 20% 1-octene having become incorporated in the resulting copolymer at 90 °C.

Introduction

The bridged cyclopentadienyl/amido group 4 metal complexes resemble in many respects their group 4 *ansa*-metallocene relatives.[1,2] Electronically, the amido group acts as a σ- and π-donor, simulating to some extent a cyclopentadienyl ligand. Probably related to this electronic similarity, such compounds can serve as components of very active homogeneous Ziegler−Natta catalysts for 1-alkene polymerization. The linked Cp/amido systems are especially useful for a variety of copolymerization reactions and have found important application in this respect.[3−6]

A variety of linkers have been reported to connect the Cp with the amido ligand in these systems, such as −$(CH_2)_n$−, with n = 2 or 3,[7] but the vast majority of the systems that have found practical application have been derived from Bercaw and Shapiro's original dimethylsilandiyl-bridged Cp*/N−CMe_3 ligand (**1**, see Chart 1).[8,9] The [Cp*−$SiMe_2$−NR]-based titanium and zirconium "constrained geometry" Ziegler−Natta catalysts have found wide application especially in ethene/1-alkene copolymerization reactions.[2]

Several variations at the original [Cp*−$SiMe_2$−NR]M framework have been reported over the years,[10−12] but only surpris-

* To whom correspondence should be addressed.
[†] Universität Münster.
[§] Universität Zürich, DFT calculations.
[‡] X-ray crystal structure analyses.

(1) Review: Brintzinger, H.-H.; Mülhaupt, R.; Fischer, D.; Rieger, B.; Waymouth, R. *Angew. Chem.* **1995**, *107*, 1255−1283; *Angew. Chem., Int. Ed. Engl.* **1995**, *34*, 1143−1170.
(2) Reviews: (a) McKnight, A. L.; Waymouth, R. M. *Chem. Rev.* **1998**, *98*, 2587−2598. See also: (b) Okuda, J.; Eberle, T. Half-Sandwich Complexes as Metallocene Analogues. In *Metallocenes − Synthesis, Reactivity, Applications;* Togni, A., Haltermann, R. L., Eds.; Wiley-VCH: Weinheim, 1998; Vol. 1, pp 415−453.
(3) Stevens, J. C.; Timmers, F. J.; Wilson, D. R.; Schmidt, G. F.; Nickias, P. N.; Rosen, R. K.; Knight, G. W.; Lai, S. Eur. Patent Appl. EP 416815-A2, 1991 (Dow Chemical Co.). Stevens, J. C. *Stud. Surf. Sci. Catal*. **1996**, *101*, 11−20.
(4) Canich, J. M. Eur. Patent Appl. EP 420436-A1, 1991 (Exxon Chemical Co.). Canich, J. M.; Hlatky, G. G.; Turner, H. W. PCT Appl. WO 92−00333, 1992.
(5) Pannell, R. B.; Canich, J. M.; Hlatky, G. G. PCT Int. Appl. WO 94/00500, 1994 (Exxon Chemical Co.). Canich, J. M. PCT Int. Appl. WO 96/00244, 1996 (Exxon Chemical Co.). Devore, D. D.; Crawford, L. H.; Stevens, J. C.; Timmers, F. J.; Mussell, R. D.; Wilson, D. R.; Rosen, R. K. PCT Int. Appl. WO 95/00526, 1995 (Dow Chemical Co.). Nickias, P. N.; McAdon, M. H.; Patton, J. T. PCT Int. Appl. WO 97/15583, 1997 (Dow Chemical Co.).
(6) Xu, G. *Macromolecules* **1998**, *31*, 2395−2402.
(7) Hughes, A. K.; Meetsma, A.; Teuben, J. H. *Organometallics* **1993**, *12*, 1936−1945. Dias, H. V. R.; Wang, Z.; Bott, S. G. *J. Organomet. Chem.* **1996**, *508*, 91−99. Sinnema, P.-J.; van der Veen, L.; Speck, A. L.; Veldman, N.; Teuben, J. H. *Organometallics* **1997**, *16*, 4245−4247. Foster, P.; Chien, J. C. W.; Rausch, M. D. *J. Organomet. Chem.* **1997**, *545/6*, 35−38. Schwink, L.; Knochel, P.; Eberle, T.; Okuda, J. *Organometallics* **1998**, *17*, 7−9. Gomes, P. T.; Green, M. L. H.; Martins, A. M. *J. Organomet. Chem.* **1998**, *551*, 133−138. van Leusen, D.; Beetstra, D. J.; Hessen, B.; Teuben, J. H. *Organometallics* **2000**, *19*, 4084−4089.
(8) Piers, W. E.; Shapiro, P. J.; Bunel, E. E.; Bercaw, J. E. *Synlett* **1990**, *2*, 74−84. Shapiro, P. J.; Bunel, E. E.; Schaefer, W. P.; Bercaw, J. E. *Organometallics* **1990**, *9*, 867−869. Shapiro, P. J.; Cotter, W. D.; Schaefer, W. P.; Labinger, J. A.; Bercaw, J. E. *J. Am. Chem. Soc.* **1994**, *116*, 4623−4640.
(9) Okuda, J. *Chem. Ber.* **1990**, *123*, 1649−1651.
(10) Carpenetti, D. W.; Kloppenburg, L.; Kupec, J. T.; Petersen, J. L. *Organometallics* **1996**, *15*, 1572−1581. Amor, F.; Okuda, J. *J. Organomet. Chem.* **1996**, *520*, 245−248. Okuda, J.; Eberle, T.; Spaniol, T. P. *Chem. Ber.* **1997**, *130*, 209−215.

10.1021/ja010943b CCC: $22.00

Chart 1 Examples of "CpSiN", "CpCN", and "CpCP" Group 4 Metal Constrained Geometry Ziegler−Natta Catalyst Precursors

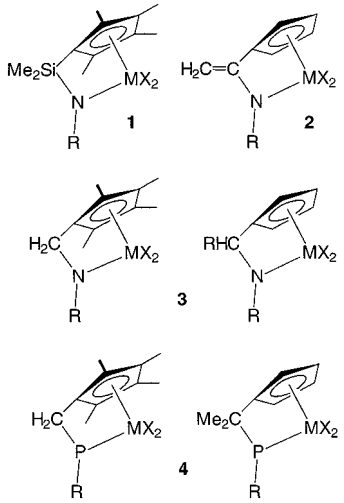

ingly few examples of general variations of groups within this given type of ligand framework have been described. In contrast to the numerous "CpSiN"MX_2 examples (**1**), only very few related "CpCN"MX_2 systems have become known so far, where a C_1 instead of the ubiquitous Si_1 linker is bridging the Cp and amido moiety inside this general ligand system. We had reported a first such example, the sp^2-C_1 bridged system **2,** a few years ago[13] and just recently have described two rather general synthetic pathways, which to our knowledge are the first examples of related sp^3-C_1 "CpCN"MX_2 catalyst systems (**3**, see Chart 1).[14] We have also recently reported a first example (**4**) of a "CpCP"MX_2 system that led to very high copolymerization catalyst activities.[14,15]

Only a few examples of hydrocarbon-bridged Cp/-oxido group 4 metal complexes have been described so far. These systems (e.g., **5a**, **5b**)[16] contain C_2- or C_3-carbon bridges (see Chart 2).[17,18] The oxygen analogues of the original "CpSiN"MX_2 systems, the "CpSiO"MX_2 complexes (**6**), were prepared and

Chart 2 Monomeric Structures of C_2- and C_3-linked Cp/-Oxido Group 4 Metal Complexes and Dimeric Structures Found for the "CpSiO"MX_2 Systems

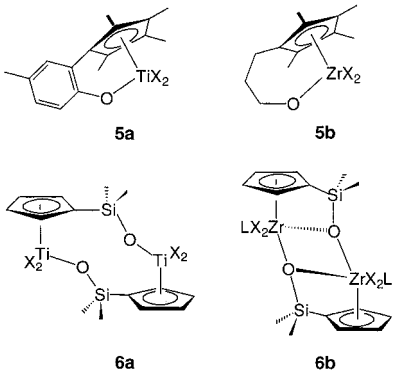

described by Ciruelos et al. However, they are not monomeric but exhibit dimeric structures in which the two group 4 metal centers are bridged by the $[Cp-SiMe_2-O]^{2-}$ ligand systems.[19] Bridging μ_3-O atoms are found in the case of the zirconium system,[20] remotely related to the situation observed in Sharpless catalyst precursors.[21] To the best of our knowledge, neither of these systems seems to have been used for the generation of active olefin homo- or copolymerization Ziegler−Natta catalysts so far.

We have now prepared the first examples of the new "CpCO"MX_2 complexes. The two systems (M = Ti, Zr) each contain a sp^2-C_1 linker between the Cp moiety and the oxygen atom of the formally dianionic ligand. The general synthetic pathway to such systems is described in this paper, along with their structural characterization and a theoretical analysis regarding their potential association behavior (monomer/dimer question). Finally, reactive Ziegler−Natta catalyst systems based on these new "CpCO"MX_2 complexes **7** were generated and tested in alkene homo- and copolymerization reactions.

Results and Discussion

Synthesis and Structural Characterization of the "CpCO"MX_2 Complexes. We used two starting materials in the course of developing a "CpCO" ligand synthesis that were both described by Hafner et al. many years ago. Formylcyclopentadienylsodium (**8a**) was prepared by treatment of CpNa with ethylformiate in boiling THF.[22,23] We first tried to synthesize

(11) du Plooy, K. E.; Moll, U.; Wocadlo, S.; Massa, W.; Okuda, J. *Organometallics* **1995**, *14*, 3129−3131. Okuda, J.; du Plooy, K. E.; Massa, W.; Kang, H.-C.; Rose, U. *Chem. Ber*. **1996**, *129*, 275−277. Okuda, J.; Verch, S.; Spaniol, T. P.; Stürmer, R. *Chem. Ber.* **1996**, *129*, 1429−1431. Amor, A.; Spaniol, T. P.; Okuda, J. *Organometallics* **1997**, *16*, 4765−4767. Brown, S. J.; Gao, X.; Harrison, D. G.; Koch, L.; Spence, R. E. v. H.; Yap, G. P. A. *Organometallics* **1998**, *17*, 5445−5447. Amor, F.; Butt, A.; du Plooy, K. E.; Spaniol, T. P.; Okuda, J. *Organometallics* **1998**, *17*, 5836−5849. Feng, S.; Klosin, J.; Krüper, W. J., Jr.; McAdon, M. H.; Neithamer, D. R.; Nickias, P. N.; Patton, J. T.; Wilson, D. R.; Abbond, K. A.; Stern, C. L. *Organometallics* **1999**, *18*, 1159−1167. Ashe, A. J., III; Fang, X.; Kampf, J. W.; *Organometallics* **1999**, *18*, 1363−1365. Galan-Fereres, M.; Koch, T.; Hey-Hawkins, E.; Eisen, M. S. *J. Organomet. Chem*. **1999**, *580*, 145−155. Okuda, J.; Eberle, T.; Spaniol, T. P.; Piquet-Fauré, V. *J. Organomet. Chem*. **1999**, *591*, 127−137. Juvaste, H.; Pakkanen, T. T.; Iiskola, E. I. *Organometallics* **2000**, *19*, 1729−1733. Gentil, S.; Pirio, N.; Meunier, P.; Gallucci, J. C.; Schloss, J. D.; Paquette, L. A. *Organometallics* **2000**, *19*, 4169−4172.
(12) Chen, Y.-X.; Marks, T. J. *Organometallics* **1997**, *16*, 3649−3657. Chen, Y.-X.; Fu, P.-F.; Stern, C. L.; Marks, T. J. *Organometallics* **1997**, *16*, 5958−5963. Lanza, G.; Fragalà, I. L.; Marks, T. J. *J. Am. Chem. Soc*. **1998**, *120*, 8257−8258.
(13) Duda, L.; Erker, G.; Fröhlich, R.; Zippel, F. *Eur. J. Inorg. Chem*. **1998**, 1153−1162.
(14) Kunz, K.; Erker, G.; Döring, S.; Fröhlich, R.; Kehr, G. *J. Am. Chem. Soc*. **2001**, *123*, 6181−6182.
(15) For publications concerning synthetic approaches to related ligand systems see, e.g., Heidemann, T.; Jutzi, P. *Synthesis* **1994**, 777−778. Koch, T.; Blaurock, S.; Somoza, F. B., Jr.; Voigt, A.; Kirmse, R.; Hey-Hawkins, E. *Organometallics* **2000**, *19*, 2556−2563.
(16) Chen, Y.; Fu, P.; Stern, C. L.; Marks, T. J. *Organometallics* **1997**, *16*, 5958−5963.
(17) Gielens, E. E. C. G.; Tiesnitsch, J. Y.; Hessen, B.; Teuben, J. H. *Organometallics* **1998**, *17*, 1652−1654.
(18) Rieger, B. *J. Organomet. Chem*. **1991**, *420*, C17−C20. Herrmann, W. A.; Morawietz, M. J. A.; Priermeier, T. *Angew. Chem*. **1994**, *106*, 2025−2028; *Angew. Chem., Int. Ed. Engl*. **1994**, *33*, 1946−1949. Trouvé, G.; Laske, D.; Meetsma, A.; Teuben, J. H. *J. Organomet. Chem*. **1996**, *511*, 255−262. Christie, S. D. R.; Man, K. W.; Whitby, R. J.; Slawin, A. M. Z. *Organometallics* **1999**, *18*, 348−359. Baker, R. W.; Wallace, B. J. *J. Chem. Soc., Chem. Commun*. **1999**, 1405−1406. Rau, A.; Schmitz, S.; Luft, G. *J. Organomet. Chem*. **2000**, *608*, 71−75.
(19) Ciruelos, S.; Cuenca, T.; Gómez-Sal, P.; Manzanero, A.; Royo, P. *Organometallics* **1995**, *14*, 177−185. Park, J. T.; Yoon, S. C.; Bae, B.-J.; Seo, W. S.; Suh, I.-H.; Han, T. K.; Park, J. R. *Organometallics* **2000**, *19*, 1269−1276.
(20) Ciruelos, S.; Cuenca, T.; Gómez, R.; Gómez-Sal, P.; Manzanero, A.; Royo, P. *Organometallics* **1996**, *15*, 5577−5585.
(21) Williams, I. D.; Pedersen, S. F.; Sharpless, K. B.; Lippard, S. J. *J. Am. Chem. Soc*. **1984**, *106*, 6430−6431. Finn, M. G.; Sharpless, K. B. In *Asymmetric Synthesis;* Morrison, J. D., Ed.; Academic Press: New York, 1985; Vol. 5, pp 247−308. Pedersen, S. F.; Dewan, J. C.; Eckman, R. R.; Sharpless, K. B. *J. Am. Chem. Soc*. **1987**, *109*, 1279−1282. Woodard, S. S.; Finn, M. G.; Sharpless, K. B. *J. Am. Chem. Soc*. **1991**, *113*, 106−113. Finn, M. G.; Sharpless, K. B. *J. Am. Chem. Soc*. **1991**, *113*, 113−126.
(22) Hafner, K.; Schulz, G.; Wagner, A. *Liebigs Ann. Chem*. **1964**, *678*, 39−52. Hafner, K.; Völpel, K. H.; Ploss, G.; König, C. *Org. Synth*. **1967**, *47*, 52−54.
(23) See also: Fujisawa, T.; Sakai, K. *Tetrahedron Lett*. **1976**, *37*, 3331−3334.

Scheme 1

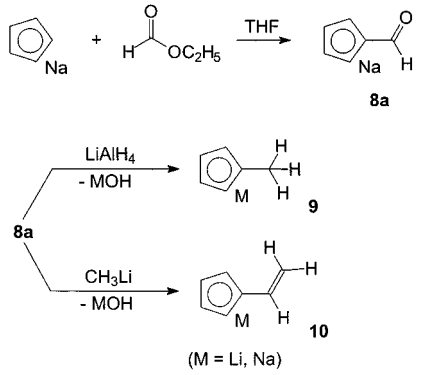

Scheme 2

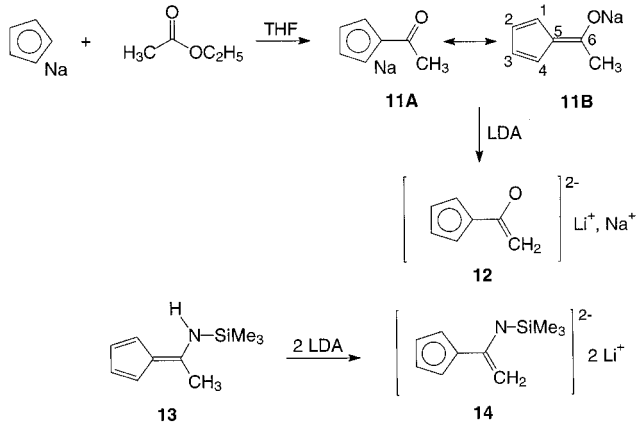

an sp^3-C_1-linked "CpCO" system, and therefore treated **8a** with $LiAlH_4$. Hydride transfer was achieved but the system was instantaneously reduced further to eventually lead to total reduction of the attached functional group to yield methylcyclopentadienyl anion.

Treatment of formylcyclopentadienylsodium with methyllithium in ether also took an unexpected course. Addition of one CH_3^- equivalent was followed by rapid MOH elimination to give the vinylcyclopentadienide system (**10**) that was identified by an NMR comparison with the literature-known vinylcyclopentadienyllithium compound.[24] Since the anticipated nucleophilic addition route did not turn out to be suited for the formation of $[Cp-CHR-O]^{2-}$ ligand systems, we tried an oxygen analogue of the synthesis that had previously been used for the preparation of the "CpCN" system **2** (see Chart 1).[13,25] The sp^2-C_1 linked Cp/amido ligand system (**14**) of **2** had been prepared by a 2-fold deprotonation reaction of the sec-aminofulvene **13** (see Scheme 2). This suggested a possible pathway to an analogous $[Cp-C(=CH_2)-O]^{2-}$ ligand system to be started from acetylcyclopentadienyl monoanion. The starting material (**11**) was prepared according to Hafner et al. by treatment of CpNa with ethyl acetate.[22] The resulting product **11** was characterized by X-ray diffraction (identical to the one previously reported by Rogers et al.[26]). The X-ray crystal structure analysis had revealed a pronounced fulvene character of **11**. It is characterized by short C1−C2 (1.370(2) Å) and C3−C4 (1.372(2) Å) bonds that are connected by a markedly longer C2−C3 bond (1.419(3) Å). The C5−C6 bond length of the exocyclic enolate-type functionality amounts to 1.417(2) Å, and the adjacent C6−O bond length is 1.253(2) Å. These values indicate a suitable description by mesomeric fulvenolate (**11A**) and acetylcyclopentadienide-type (**11B**) structures.[27] The sodium cations in the lattice show electrostatic contacts to oxygen and to the carbon atoms of the Cp ring (for details see ref 26 and the Supporting Information).

Scheme 3

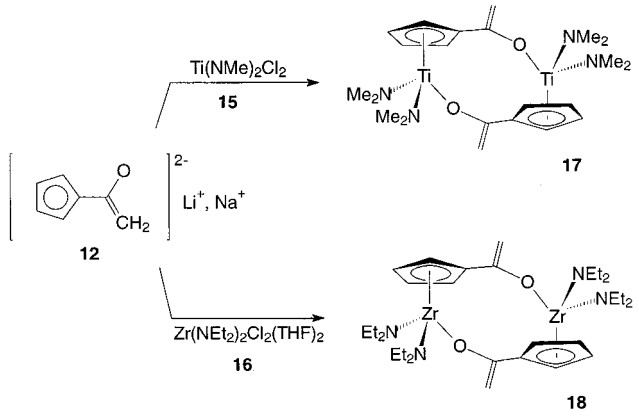

Deprotonation of **11** at the 6-CH_3 group can be achieved readily as was expected from these structural results. Treatment of **11** with LDA in tetrahydrofuran at room temperature cleanly gave the dianionic reagent **12**, which was then reacted with $Ti(NMe_2)_2Cl_2$ (**15**) in tetrahydrofuran. After 2 h at ambient temperature, the metathetical exchange reaction was complete and the organometallic vinylidene-linked Cp/-oxido titanium product (**17**) was isolated as a yellowish solid in >70% yield. It is characterized by ^{1}H NMR features at δ 4.33 and 3.85 of the vinylidene protons[29] and a set of ^{13}C NMR signals at δ 129.1 (ipso-C), 112.5, and 109.6 of the monosubstituted η^5-Cp ring and δ 162.6 (quart. C) and 88.0 of the vinylidene linker.

The reaction of **12** with the reagent $Zr(NEt_2)Cl_2(THF)_2$ (**16**) proceeded analogously and furnished the corresponding sp^2-C_1-linked Cp/-oxido zirconium complex (**18**) in ca. 75% yield. The ^{1}H NMR spectrum shows a characteristic set of α- and β-Cp resonances at δ 6.36 and 6.25 aside from the $C{=}CH_2$ resonances at δ 4.39 and 3.98. The ^{1}H NMR spectrum of **18** shows a single set of $-N(C_2H_5)_2$ signals (CH_3: triplet at δ 1.04), with a diastereotopic splitting of its methylene resonances (AB part of an ABX_3 system) because of the prochirality of complex **18**. Complex **18** is dimeric in solution. This was shown by cryoscopy in benzene (n_{exp} = 2.2). The dimeric, dimetallic composition of these complexes was confirmed by an X-ray crystal structure analysis of the zirconium complex **18**. Single crystals were obtained at −20 °C from a solution of the complex in dichloromethane. In the crystal, there are two almost identical molecules in the unit cell; the two zirconium atoms of each

(24) Macomber, D. W.; Hart, W. P.; Rausch, M. D.; Priester, R. D.; Pittmann, C. U. *J. Am. Chem. Soc.* **1982**, *104*, 884−886.
(25) Kunz, D.; Fröhlich, R.; Erker, G. *Organometallics* **2001**, *20*, 572−574.
(26) Rogers, R. D.; Atwood, J. L.; Rausch, M. D.; Macomber, D. W.; Hart, W. P. *J. Organomet. Chem.* **1982**, *238*, 79−85.
(27) For related effects in Cp-formidoyl anion systems see, e.g., Kunz, K.; Erker, G.; Kehr, G.; Fröhlich, R. *Organometallics* **2001**, *20*, 392−400.
(28) Alexandratos, S.; Streitwieser, A., Jr.; Schaefer, H. F., III. *J. Am. Chem. Soc.* **1976**, *98*, 7959−7962. Jemmis, E. D.; Schleyer, P. v. R. *J. Am. Chem. Soc.* **1982**, *104*, 4781−4788. Setzer, W. N.; Schleyer, P. v. R. *Adv. Organomet. Chem.* **1985**, *24*, 353−451. Lambert, C.; Schleyer, P. v. R. *Angew. Chem.* **1994**, *106*, 1187−1199; *Angew. Chem., Int. Ed. Engl.* **1994**, *33*, 1129−1141. *Lithium Chemistry, A Theoretical and Experimental Overview*; Sapse, A.-M., Schleyer, P. v. R., Eds.; Wiley: New York, 1995; and references therein.
(29) For a comparison with nonbridged group 4 metal enolate complexes see Spaether, W.; Klass, K.; Erker, G.; Zippel, F.; Fröhlich, R. *Chem. Eur. J.* **1998**, *4*, 1411−1417.

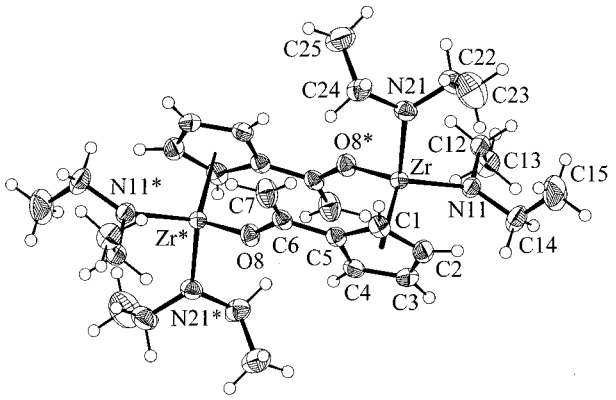

Figure 1. A view of the dimeric molecular structure of the "CpCO"Zr complex **18** in the crystal. Selected bond lengths (Å), angles, and dihedral angles (°): Zr1a−O8a* 1.996(1), Zr1b−O8b* 1.993(1), Zr1a−N11a 2.032(1), Zr1b−N11b 2.036(1), Zr1a−N21a 2.042(1), Zr1b−N21b 2.050(1), Zr1a−C_{Cp} 2.522(2)−2.563(2), Zr1b−C_{Cp} 2.510(2)−2.553(2), C5a−C6a 1.477(2), C5b−C6b 1.474(2), C6a−C7a 1.326(3), C6b−C7b 1.327(3), C6a−O8a 1.341(2), C6b−O8b 1.342(2); O8a*−Zr1a−N11a 111.09(5), O8b*−Zr1b−N11b 109.85(6), O8a*−Zr1a−N21a 102.37(6), O8b*−Zr1b−N21b 103.85(6), N11a−Zr1a−N21a 101.23(6), N11b−Zr1b−N21b 100.95(6), Zr1a*−O8a−C6a 151.6(1), Zr1b*−O8b−C6b 153.1(1), O8a−C6a−C7a 122.3(2), O8b−C6b−C7b 122.4(2), O8a−C6a−C5a 114.3(1), O8b−C6b−C5b 114.4(2), C7a−C6a−C5a 123.4(2), C7b−C6b−C5b 123.2(2); C5a−C6a−O8a−Zr1a* 125.3(2), C5b−C6b−O8b−Zr1b*−125.2(2), C7a−C6a−O8a−Zr1a* −56.3(3); C7b−C6b−O8b−Zr1b* 56.3(3).

molecule are connected by two μ-[η^5:κO−Cp−C(=CH_2)−O] ligands in an arrangement exhibiting overall inversion symmetry. The symmetry-equivalent [Cp−C(=CH_2)−O] ligand systems are each almost coplanar. The C_5H_4-moiety is uniformly η^5-coordinated to the zirconium atom. The Cp(centroid)−Zr distance in complex **18** amounts to 2.244 Å (molecule A). The exocyclic C6−C7 double bond (1.326(3) Å) is not involved in the bonding to the metal. The adjacent C5−C6 bond length amounts to 1.477(2) Å, and the C6−O bond length is 1.341(2) Å. The Zr−O bond is short at 1.996(1) Å, in fact much shorter than observed in Royo's dinuclear "CpSiO"Zr complex **6b** (2.207 Å, see Chart 2). This indicates pronounced oxygen to zirconium π-back-bonding in **18**, similar as it is often observed in large-ring Zr (and Ti) alkoxide complexes[30] and in μ-oxo group 4 metallocenes.[31] Consequently, the Zr−O−C6 angle in complex **18** is substantially enlarged at 151.6(1)°. The overall complex framework is bent at O8. The corresponding dihedral angle θ(C5−C6−O8−Zr) amounts to 125.3(2)°. The Zr−N(Et)$_2$ conditions are similar in length to each other (Zr−N11 2.032(1) Å, Zr−N21 2.042(1) Å). Inside the distorted "piano-stool"-type structure, their N−Zr−Cp angles are quite different, however, (N21−Zr−Cp(centroid) 119.6°, N11−Zr−Cp(centroid) 109.4°). The O−Zr−Cp(centroid) angle in **18** amounts to 112.5°.

DFT Calculations. The monomer/dimer problem of the structures of the "CpSiN", "CpSiO", "CpCN", and "CpCO"Zr constrained geometry systems was approached by means of a computational chemistry study using DFT calculations.

First, a series of mononuclear model compounds was investigated. The monomeric local minimum structures of the

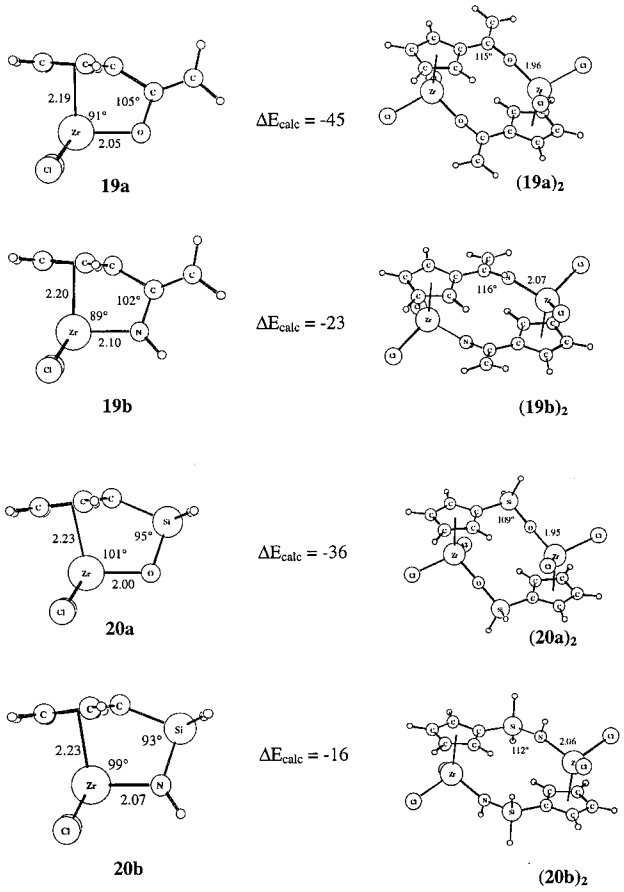

Figure 2. A comparison between the DFT calculated monomeric and dimeric model compounds **19** (sp^2-C_1-bridged) and **20** (Si-bridged).

hypothetical molecules were calculated. There are a few points that should be noted. The monomeric compounds all seem to have a considerable strain accumulated in their structural frameworks. For the system [Cp−C(=CH_2)−O]$ZrCl_2$ (**19a**, (Cp) see Figure 2) this becomes evident by a decreased C(Cp)−C−O angle inside the bridge from an expected value of 120° to a mere 105°. At the same time, the Cp(centroid)−Zr−O angle in the monomer **19a** amounts to only 91°. Similar characteristic features were obtained from the DFT calculation of the hypothetical nitrogen-containing analogue [Cp−C(=CH_2)−NH]-$ZrCl_2$ (**19b**, see Figure 2). The respective dimethylsilandiyl-bridged complexes show similar features. Here, angles at the bridging silicon atom are smaller whereas the corresponding angle at the central metal atom is increased (e.g., **20a**: C(Cp)−Si−O 95°, Cp(centroid)−Zr−O 101°, see also Figure 2).

Next, we calculated the corresponding monocyclic dimeric structures (**19a,b**)$_2$ and (**20a,b**)$_2$. All four dimers of these model compounds were energetically more favorable (negative energy difference ΔE) than their respective monomers. The bridging group 14 atom had relaxed to endocyclic bond angles (e.g., (**19a**)$_2$: C(Cp)−C−O 115°, for additional values see Figure 2) that indicate a considerably less strained ligand framework in these complexes. There seems to be an additional effect in the oxygen-containing compound that leads to an increased energetic preference of the dimers: in (**19a**)$_2$ the calculated Zr−O bond length (1.96 Å) is markedly shorter than in the monomer **19a** (2.05 Å), whereas this effect seems to be negligible in the **19b** (Zr−N 2.10 Å) to (**19b**)$_2$ (Zr−N 2.07 Å) transition in the nitrogen-containing model system. In all four calculated model

(30) Erker, G.; Dehnicke, S.; Rump, M.; Krüger, C.; Werner, S.; Nolte, M. *Angew. Chem.* **1991**, *103*, 1371−1373; *Angew. Chem., Int. Ed. Engl.* **1991**, *30*, 1349−1351. Spaether, W.; Erker, G.; Rump, M.; Krüger, C.; Kuhnigk, J. *Organometallics* **1995**, *14*, 2621−2623.
(31) Erker, G.; Dorf, U.; Krüger, C.; Tsay, Y.-H. *Organometallics* **1987**, *6*, 680−682 and references therein.

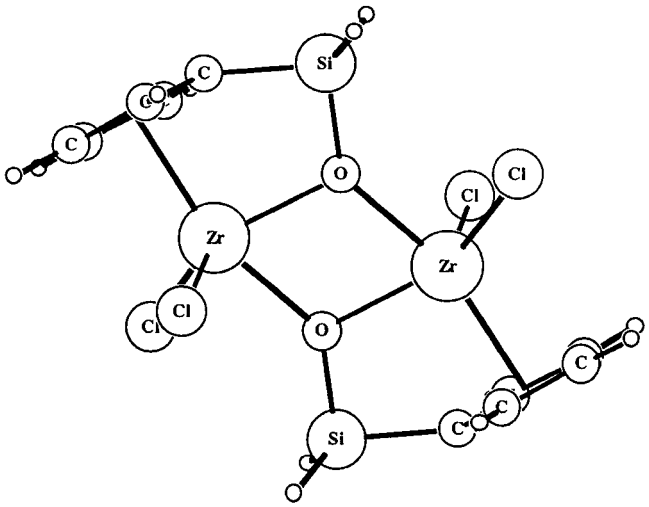

Figure 3. DFT calculated isomeric dimetallatricyclic structural alternative (**20a**)$_2$′.

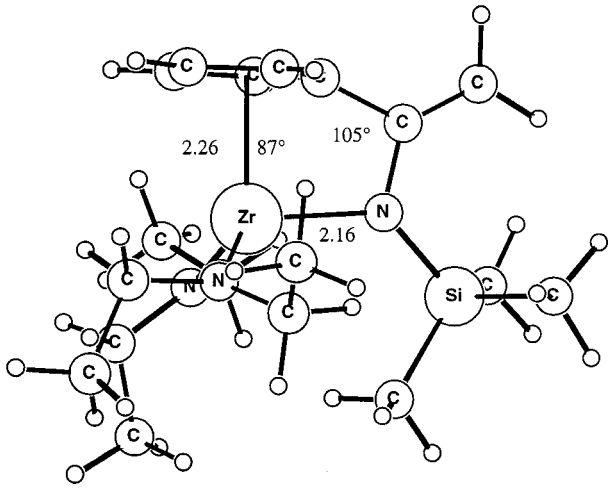

Figure 4. DFT calculated monomeric structure of the "constrained geometry" complex **2a**.

cases, the dimeric structures seem to be favored energetically, but the thermodynamic preference for dimer formation is much more pronounced for the oxygen-containing examples than for the related nitrogen systems. According to this calculation, the oxygen-bridged dimer (**19a**)$_2$ is favored over its monomers (2 × **19a**) by $\Delta E = -45$ kcal mol^{-1}. For the nitrogen system 2 × **19b** → (**19b**)$_2$, the dimerization energy has dropped considerably to $\Delta E = -23$ kcal mol^{-1}. The relative thermodynamic preference of the silicon-containing dimers is slightly smaller with a similar ΔE between the oxygen- and nitrogen-containing pairs (the calculated ΔE values are given in Figure 2).

We also calculated for one example the dimetallatricyclic structural alternative (**20a**)$_2$′ (see Figure 3). Its DFT calculated energy [ΔE (2 × **20a**) − (**20a**)$_2$′ = −35 kcal mol^{-1}] relative to the monomeric model compound **20a** is only marginally different from the monocyclic dimer (**20a**)$_2$ that is depicted in Figure 2. The metallatricyclic structure seems not to be a favored alternative in these systems. That such an example (**6b**, see Chart 2) was observed by X-ray diffraction may therefore have been determined by crystal packing forces.

We then calculated two systems that could be compared to experimentally determined X-ray crystal structure analyses. The DFT minimum structure of our previously described first example of a "CpCN"ZrX_2 system with a sp^2-C$_1$ linker between the Cp and the amido moiety, the complex [Cp−C(=CH$_2$)−NSiMe$_3$](NEt$_2$)$_2$ (**2a**)[13] is depicted in Figure 4. The calculated dimerization energy is $\Delta E \leq 2$ kcal mol^{-1} (i.e., 2 × **2a** → (**2a**)$_2$) which makes it likely that the constrained geometry complex **2a** in solution favors a monomeric structure (ΔG slightly positive) as it is typically observed for the many N-substituted Cp/amido-constrained geometry group 4 complexes that have become known so far.

The situation is markedly different in the calculation of the real "CpCO"ZrX_2 system **18**. The DFT calculated global minimum is a dimetallic monocyclic structure that is almost identical to the observed X-ray structure of **18**. The calculated C(Cp)−C−O angle is 115°, which is the same as experimentally observed. The Zr−O−C angle in the calculated structure amounts to 152°, the experimental value is 151.6(1)°. The calculated Zr−O bond length is 2.01, to be compared with the experimental value of 1.996(1) Å. Our DFT calculation revealed a dimerization energy of $\Delta E = -41$ kcal mol^{-1} in favor of the calculated (and experimentally observed) dimeric structure **18**. So far, we have only considered steric effects in the analysis of the monomer/dimer problem. We now have a closer look at specific orbital interactions, not only to get a more detailed understanding of this question, but also to elucidate the differences between the constrained oxygen- and nitrogen-based systems. To this end, we performed a fragment orbital analysis for a series of simplified model compounds CpZrCl$_2$X **21a**, **22a** (X = OH) and **21b**, **22b** (X = NH$_2$), depicted in Scheme 4.

The geometries of these complexes were modeled from the optimized structures of complexes **19a**, (**19a**)$_2$ for **21a**, **22a**, and **19b**, (**19b**)$_2$ for **21b**, **22b**, respectively. The orbital interaction for the formation of the Zr−X bond was determined by analysis of the bond-forming reaction of the cationic metal fragment and the negatively charged ligand. The important orbital interactions are displayed in Chart 3 and are classified according to C$_s$-symmetry as 1a′, 2a′, and 1a″.

This allows for a partitioning of the orbital interaction energies ΔE_{int} into two components $\Delta E(\sigma)$ and $\Delta E(\pi)$, derived from symmetric and antisymmetric interactions, respectively. The results of the analysis are collected in Table 1. If we compare the analysis for complexes **21a** and **21b**, which possess the coordination geometry of the constrained monomers, we see that the Zr−N bond has a remarkably stronger π-component and a somewhat stronger σ-component, when compared to the Zr−O bond. This supports the notion that the amido group represents the better π donor. Changing the coordination geometry to that of the constrained dimers, we find for the Zr−O bond a lower σ- as well as π-component. This results in an overall weaker orbital interaction energy for the Zr−O bond in the dimer. When comparing the amido complexes **21b** and **22b**, we find a remarkable drop in π-interaction energy and a slight increase in the σ-component. This change in orbital interaction results from the change of the coordination geometry around the N-atom (compare Chart 3), which causes a reduced 1a″ and an increased 2a′ interaction.

The fact that in both cases X = NH$_2$ and X = OH, CpZrCl$_2$X complexes with the coordination geometry of the constrained monomers show the stronger orbital interaction, supports the notion that the formation of the dimer is to a major extent driven

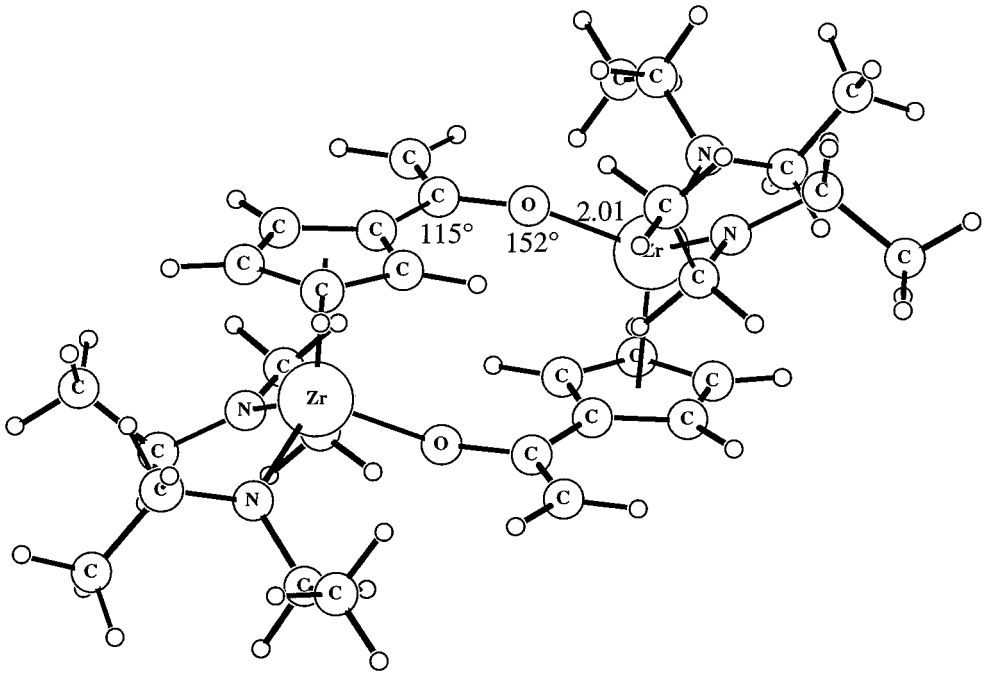

Figure 5. Calculated cyclodimeric structure of the "CpCO"$Zr(NEt_2)_2$ complex **18**.

Scheme 4

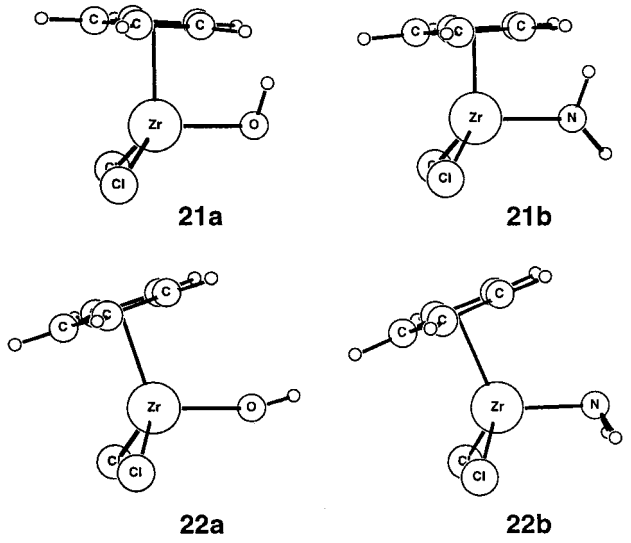

by the release of steric strain. The fact that under formation of the dimer the drop in orbital energy is significantly larger for the Zr−N bond than for the Zr−O bond might provide one explanation why the dimerization of **19a** is energetically more favorable than that of **19b**. The reason here was a significant reduction of π-donation under pyramidalization of the N-center. The strong π-type interaction of orbital 1a″ is transformed into a σ-type interaction 2a′.

The complexes **17** (Ti) and **18** (Zr) were used as transition-metal components for the generation of active homogeneous Ziegler−Natta catalyst systems (see below). It must be assumed that the respective $[M]-CH_3^+$ cation systems serve as the catalytically active species after activation with methylalumoxane (MAO). Olefin insertion into the $M-CH_3$ σ-bond then starts the alkene polymerization process. To find out about possible differences in the alkene polymerization features between the potential mononuclear and dinuclear "CpCO"$M-R^+$ Ziegler−

Chart 3 Main Orbital Interactions Characterizing the $ZrCpR_2-X$ Bond (X = OH, NH_2)

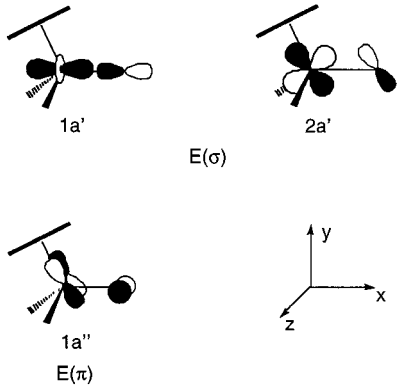

Scheme 5

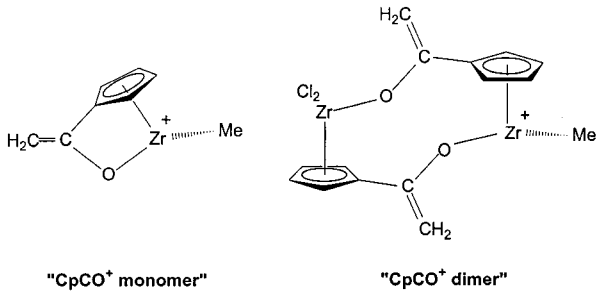

Natta catalysts, we carried out DFT calculations of the ethene insertion reaction of the respective cationic "$CpCO^+$-monomer" and "$CpCO^+$-dimer" catalyst models (see Scheme 5). Such ethene insertion profiles have been already studied for some metallocene cations and various other Cp-containing Ziegler−Natta catalyst systems.[32] In the calculation, a molecule of ethylene was placed into the vicinity of the $Zr-CH_3$ bond of the respective model systems. Different values of the distance

(32) Woo, T. K.; Fan, L.; Ziegler, T. *Organometallics* **1994**, *13*, 2252−2261.

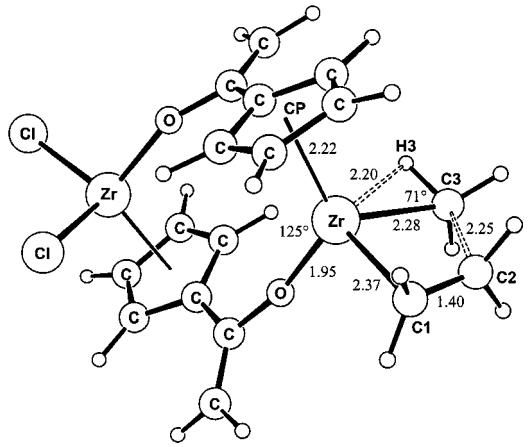

Figure 6. DFT calculated transition state of ethene insertion at the ["$CpCO^+$-dimer"]$Zr-CH_3$ model system.

Table 1. Orbital Interaction Energies (in eV) for the Zr−X Bond of Model Compounds $CpZrCl_2X$ **21a**, **22a** (X = HO) and **21b**, **22b** (X = H_2N)

	21a	21b	22a	22b
$\Delta E(\sigma)$	−3.09	−3.24	−2.69	−3.62
$\Delta E(\pi)$	−1.43	−2.11	−1.25	−0.85
ΔE_{int}	−4.52	−5.35	−3.94	−4.47

between one ethylene terminus and the "active" $-CH_3$ carbon atom (defined as the reaction coordinate R_{cc}) were successively kept fixed while all other structural parameters were fully optimized. The transition states described below were calculated from the geometries corresponding to maxima along the ethylene insertion hypersurfaces. Figure 6 depicts the ethylene insertion transition state $\mathbf{TS_{di}}$ of the "$CpCO^+$-dimer" catalyst system (dihedral angles O−CP(centroid)−Zr−C1 = −124.6°, O−CP−Zr−C2 = −158.4°, O−CP−Zr−C3 = +140.4°, O−Zr−CP−C6 = −55.9°), whereas Figure 7 shows two projections of the transition state $\mathbf{TS_{mo}}$ of the "$CpCO^+$-monomer" system (with the corresponding dihedral angles amounting to −101.7°, −113.2°, +130.3°, and −1.1°).

Figure 8 shows a schematic representation of the ethene insertion reaction at these two model systems along the R_{cc} reaction coordinate, revealing that the DFT calculated energetic features of ethene insertion at the mononuclear and dinuclear "CpCO"$Zr-CH_3^+$ catalysts are very similar. Actually, it appears from our model calculation that ethene insertion at the dinuclear system (at the cationic state) is even slightly more favorable, although the energetic differences between the two model systems are minute.

Polymerization Reactions. We have obtained cumulated evidence by our experimental work and the theoretical analysis that a dimeric structure is energetically favored for the "CpCO"ZrX_2 system **18**. Thus, this system structurally behaves different from our related $[Cp-C(=CH_2)NR]ZrX_2$ system (**2**), from our new recently reported $[Cp-CHR-NR]MX_2$ (M = Ti, Zr) systems **3,** and from the many examples of the original dialkylsilandiyl-linked Cp/amido group 4 metal systems $[Cp-SiR_2-NR]MX_2$ (**1**), for which the term "constrained geometry" catalysts was actually coined. The dimetallic framework of **18** is lacking the steric constraints that may be characteristic for the above-mentioned class of homogeneous Ziegler−Natta catalyst systems. Therefore, is was important to learn about the catalytic features of **18** (when treated with a suitable activator component) and to note whether such a system would behave markedly different from a known conventional "constrained geometry" Ziegler−Natta catalyst system.[33]

The ["CpCO"$Ti(NMe_2)_2$]$_2$ complex **17** was activated by treatment with methylalumoxane (MAO)[34] in toluene solution (Al:Ti ratio > 400, see Table 2). Ethene was polymerized during 1 h at 60 °C to give polyethylene (T_m = 125 °C) with a moderate catalyst activity of a = 44 g PE/mmol [Ti]·h·bar. The analogous zirconium Ziegler−Natta catalyst system **18**/MAO is also active in ethene polymerization. At 65 °C it shows similar catalyst activities (see Table 2). For a comparison, two conventional "CpSiN"ZrX_2 systems [**1a** (X = Cl), **1b** (X = NMe_2)] were treated with MAO and were used in ethene polymerization as well (see Table 2). Polyethylene formation at the respective $[Cp^*-SiMe_2-NCMe_3]Zr(NMe_2)_2$ (**1b**)/MAO catalyst took place at 60 °C with a slightly lower activity as compared to the ["CpCO"$M(NR_2)_2$]$_2$/MAO catalysts (see Table 2).

The ["CpCO"$Zr(NEt_2)_2$]$_2$ (**18**)/MAO Ziegler−Natta catalyst system turned out to be well suited for effective ethene/1-octene copolymer formation. In a typical experiment (see Table 2, entry 8), statistical polyethylene-*co*-poly-1-octene that contained ca. 20% of the C_8−α-olefin incorporated was formed at 90 °C in toluene/50% 1-octene solution with a 1 bar ethene pressure. Figure 9 shows a characteristic section of the ^{13}C NMR spectrum of the copolymer.[35] This oily copolymer was obtained with catalyst activities ranging from a = 100 to 200 (see Table 2). The titanium Ziegler−Natta catalyst analogue **17**/MAO gives a similar ethene/1-octene copolymer, and the catalyst activity is comparable. The copolymerization activities of the dimethylsilandiyl-linked "constrained geometry" catalysts are slightly higher under these conditions and lead to slightly higher 1-alkene incorporation.

We have used as additional reference systems the homogeneous Ziegler−Natta catalysts that were derived from the unbridged "piano-stool" mono-CpZr trisamide complexes **23a** and **23b** (see Chart 4).[36] Their treatment with excess MAO generated active Ziegler−Natta catalyst systems for ethene/1-octene copolymerization similar in activity to the "CpCO"ZrX_2 and the conventional "CpSiN"ZrX_2 catalysts, although a slightly lower 1-octene incorporation was observed.

Conclusions

This study shows that the synthetic route that was developed for the preparation of the first example of a "CpCN"MX_2 catalyst precursor, the complex $[Cp-C(=CH_2)-NSiMe_3]Zr(NEt_2)_2$,[13] can be applied for an analogous synthetic pathway to a related "CpCO"MX_2 system. Deprotonation of acetylcy-

(33) We have attempted to identify potential active catalyst species in solution by ESI-MS. For that purpose, samples of the zirconium complex **18** in CD_2Cl_2 solution were treated with 10% MAO solutions in toluene (Al: Zr ≈ 2.5) at ambient temperature. The ESI-MS analysis revealed the presence of prominent Zr-containing cations with *m*/*z* centered at 833 and 704 (the dinuclear precursor species **18** has *m*/*z* 682). The exact composition and structures of these species have remained unclear so far. Products of olefin incorporation were not observed when these experiments were carried out under ethylene.

(34) Sinn, H.; Kaminsky, W. *Adv. Organomet. Chem.* **1980**, *18*, 99−149. Kaminsky, W.; Külper, K.; Brintzinger, H. H.; Wild, F. R. W. P. *Angew. Chem.* **1985**, *97*, 507−508; *Angew. Chem., Int. Ed. Engl.* **1985**, *24*, 507−508.

(35) Formal description of the copolymer ^{13}C NMR signals and their assignment was carried out according to Randall, J. C. *JMS−Rev. Macromol. Chem. Phys.* **1989**, *C29* (2 & 3), 201−317.

(36) Chandra, G.; Lappert, M. F. *J. Chem. Soc.* A **1968**, 1940. Irigoyen, A. M.; Martin, A.; Mena, M.; Palacios, F.; Yelamos, C. *J. Organomet. Chem.* **1995**, *494*, 255−259.

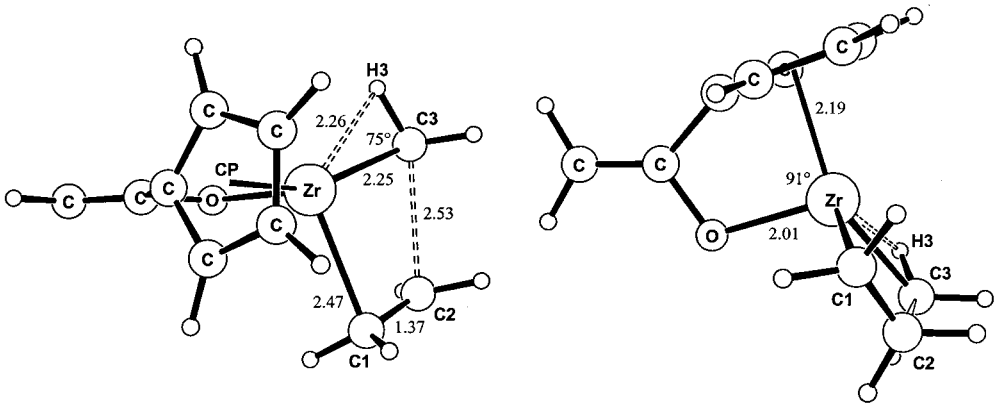

Figure 7. DFT calculated ethene insertion transition state of the $[(CpCO)Zr-CH_3]^+$ ("$CpCO^+$-monomer") system.

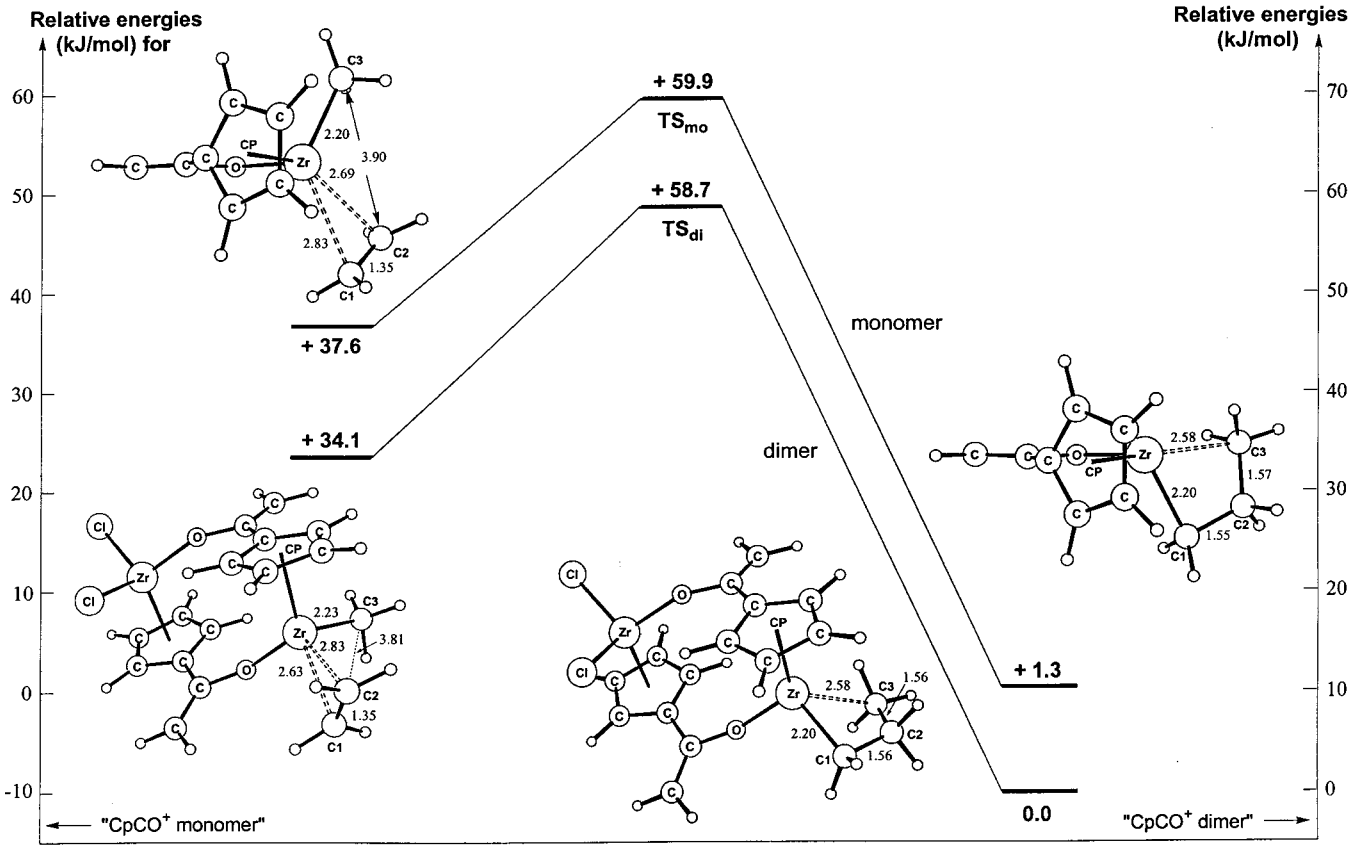

Figure 8. A comparison of the DFT calculated energy profiles of ethene insertion into the $Zr-CH_3$ bond of the "$CpCO^+$-dimer" $\mathbf{TS_{di}}$ and "$CpCO^+$-monomer" $\mathbf{TS_{mo}}$ model systems.

clopentadienide led to the formation of the $[Cp-C(=CH_2)-O]^{2-}$ ligand equivalent that could successfully be transmetalated to titanium or zirconium using the respective $Cl_2M(NR_2)_2$ reagents (M = Ti, Zr). However, the structures of the "CpCN"and the "CpCO"ZrX_2 systems turned out to be drastically different. The nitrogen-containing systems are mononuclear complexes that exhibit a "constrained" framework geometry similar as the conventional $[Cp^*-SiMe_2-NR]ZrX_2$ "constrained geometry" Ziegler–Natta catalyst precursors,[2] whereas the "CpCO"ZrX_2 system **18** has turned out to be a dimer. In this system, the $[Cp-C(=CH_2)-O]^{2-}$ ligand simply bridges between the two group 4 metal centers. Our experimental work as well as an accompanying DFT calculation shows that specific steric constraints are absent in the dimer **18**.

Nevertheless, the **18**/MAO system is an active homogeneous Ziegler–Natta catalyst that can successfully be used in the preparation of ethene/1-octene copolymers. Actually, copolymers were obtained at this dimeric "CpCO"$Zr(NEt_2)_2$ catalyst that contained up to 20% of the 1-octene monomer incorporated. The catalyst activities were only slightly lower than observed for the directly related conventional "CpSiN" catalyst system $[Cp^*-SiMe_2-NCMe_3]Zr(NMe_2)_2$/MAO. Our study cannot rule out completely that the active catalyst derived by MAO treatment of **18** is a dissociated mononuclear species, but there is accumulating evidence from our experiments as well as computations that an active dinuclear catalyst can at least successfully compete with the conventional monomers in this polymerization catalysis.

Table 2. Polymerization and Copolymerization Reactions at the **17** and **18**/MAO "CpCO" Ziegler−Natta Catalysts and Related Reference Systems

polymer	complex	catalyst, mg	Al/M	*t*, min	polymer, g	mp (% octene)	act.[a]
Ethene Polymerization at 65 °C[b]							
1[c]	**17**	18.5	430	30	3.3	125	44
2	**18**	20.0	560	45	4.2	128	48
3	**18**	10.0	1130	45	3.1	129	70
4	**1a**	17.1	680	60	2.4	125	29
5	**1b**	16.0	890	60	2.4	122	27
Ethene/1-Octene Copolymerization at 90 °C[d]							
6[e]	**17**	21.0	380	30	1.1	14	30
7	**18**	20.0	560	30	6.2	18	210
8	**18**	20.5	550	60	6.5	20	110
9	**23a**	20.0	490	60	38.5	14	550
10	**23b**	22.0	560	60	36.0	14	610
11	**1a**	18.0	750	60	28.8	20	660
12	**1b**	20.0	660	60	20.8	25	400

[a] Catalyst activities in g polymer/mmol [M]·h·bar (ethene). [b] In toluene solution, 2 bar ethene pressure. [c] At 60 °C. [d] 50% 1-octene solution in toluene, 1 bar ethene pressure. [e] 2 bar ethene pressure.

A special steric constraint effect, that was previously thought to be responsible for the excellent copolymerization performance of the well established and widely used silylene-linked Cp/amido group 4 metal Ziegler−Natta catalyst systems,[2,12] is probably not necessary for achieving almost comparably catalyst performance in the related "CpCO"Zr catalysts. It may be that the principal structural feature of the conventional Si- (or C)-linked Cp/amido group 4 metal catalysts is simply the presence of a Cp and an amido ligand in a single molecule that leads to acceptable ethene/1-alkene copolymerization catalyst properties. This is supported by the observation of the copolymerization activities of the simple unbridged Cp/amido zirconium systems **23a** and **23b**. Thus, it appears that the *general influence* of a "constrained geometry" in this general class of Ziegler−Natta copolymerization catalysts should be critically reviewed. The observations made during this study and slowly increasing evidence published elsewhere[37] seem to indicate that the steric constraints imposed by the $[^{R}Cp'-X-Y]^{2-}$ frameworks might not be a *necessary* prerequisite for achieving copolymerization activities as previously thought, although the specific catalyst performance will, of course, probably be markedly influenced if not determined by such characteristic backbone features.

Experimental Section

Reactions with organometallic compounds were carried out under argon using Schlenk-type glassware or in a glovebox. Solvents were dried and distilled under argon prior to use. For additional general information including a list of spectrometers used for physical characterization of the compounds, see ref 27. Sodium acetylcyclopentadienide (**11**) was prepared as described in the literature.[22,26] The reagents $Cl_2Ti(NMe_2)_2$ (**15**) and $Cl_2Zr(NEt_2)_2(THF)_2$ (**16**) were synthesized as previously described in the literature.[38]

Reaction of Sodium Acetylcyclopentadienide (11) with LDA, Generation of 12. A mixture of **11**·THF (1.07 g, 5.3 mmol) and LDA (560 mg, 5.3 mmol) was dissolved in 100 mL of tetrahydrofuran and then was stirred for 3 h at ambient temperature. Solvent was then removed in vacuo. The obtained solid was not completely soluble in THF. Therefore, the salt **12** was usually generated in situ for the preparation of the zirconium and titanium complexes. Spectroscopic characterization of **12**: ^{1}H NMR (THF-d_8, 200 MHz) δ 6.04, 5.61 (br, each 2H, Cp), 3.79 (br, 2H, $=CH_2$); ^{13}C NMR (THF-d_8, 50 MHz) δ 105.5, 102.5 (C_5H_4), 85.7 ($=CH_2$), both ipso-C not detected.

X-ray Crystal Structure Analysis of 11. Formula $C_7H_7ONa{\cdot}C_4H_8O$, $M = 202.22$, light yellow crystal 0.40 × 0.30 × 0.20 mm, $a = 6.659(1)$, $b = 15.979(1)$, and $c = 10.511(1)$ Å, $\beta = 92.96(1)°$, $V = 1116.9(2)$ Å^3, $\rho_{calc} = 1.203$ g cm^{-3}, $\mu = 1.13$ cm^{-1}, absorption correction via SORTAV ($0.956 \le T \le 0.978$), $Z = 4$, monoclinic, space group $P2_1/c$ (No. 14), $\lambda = 0.71073$ Å, $T = 198$ K, ω and φ scans, 10 450 reflections collected ($\pm h$, $\pm k$, $\pm l$), $[(\sin\theta)/\lambda] = 0.71$ Å^{-1}, 3393 independent ($R_{int} = 0.039$) and 2176 observed reflections [$I \ge 2\,\sigma(I)$], 165 refined parameters, $R = 0.050$, $wR^2 = 0.133$, max residual electron density 0.28 (−0.19) e Å^{-3}, THF molecule disordered, refined with split positions (0.58:0.42(1)) and additional geometrical constraints (SADI), hydrogens calculated and refined as riding atoms.

Synthesis of 17. The reagents **11**·THF (0.50 g, 2.65 mmol) and LDA (280 mg, 2.65 mmol) were mixed as solids in a Schlenk flask. THF (100 mL) was added and the mixture was dissolved at room temperature. The reaction mixture was stirred for 3 h at ambient temperature to bring the deprotonation reaction to completion. It was then added dropwise at 0 °C to a solution of $Cl_2Ti(NMe_2)_2$ (**15**, 549 mg, 2.65 mmol) in 100 mL of tetrahydrofuran. After a reaction time of 2 h, the solvent was removed in vacuo. The residue was taken up in dichloromethane and was filtered through Celite. Solvent was removed from the clear filtrate in vacuo and the product was dried in vacuo to yield 470 mg (73%) of **17**, mp 94 °C. Anal. Calcd for $C_{22}H_{36}N_4O_2Ti_2$ (484.4): C, 54.56; H, 7.49; N, 11.56. Found: C, 54.95; H, 7.54; N, 11.43%. ^{1}H NMR (CD_2Cl_2, 200 MHz): δ 6.13 (m, 8H, Cp), 4.33 and 3.85 (each br s, each 2H, $=CH_2$), 3.21 (s, 24H, NMe_2). ^{13}C NMR (THF-d_8, 50 MHz): δ 162.1 and 88.0 ($C=CH_2$), 129.1 (ipso-C of C_5H_4), 112.5 and 109.6 (C_5H_4), 49.1 ($N-CH_3$).

Synthesis of 18. Analogously as described above compound **11**·THF (1.0 g, 5.3 mmol) was deprotonated by treatment with LDA (560 mg, 5.3 mmol) in THF (100 mL) at room temperature. The in situ generated dianion equivalent **12** was then reacted with $Cl_2Zr(NEt_2)_2(THF)_2$ (2.37 g, 5.3 mmol) in THF (100 mL). Workup as described above gave 1.37 g (76%) of **18**, mp 64 °C. Anal. Calcd for $C_{30}H_{52}N_4O_2Zr_2$ (683.2): C, 52.73; H, 7.69; N, 8.20. Found: C, 53.71; H, 7.26; N, 7.61%. Cryoscopic molecular weight determination in benzene: 342 mg $\{[Cp-C(=CH_2)-O]Zr(NEt_2)_2\}_n$ in 3.65 g of benzene, equivalent to 0.27/n mol/kg gave a melting-point depression of $\delta T = K_{Kr}m_B = 0.63$ K, with K_{Kr} (benzene) = 5.12 [K·kg/mol]. This corresponds to $m_B = 0.123$ mol/kg and $n = 2.2$. ^{1}H NMR (CD_2Cl_2, 600 MHz): δ 6.36 and 6.25 (each m, each 4H, C_5H_4), 4.39 and 3.98 (each br s, each 2H, $=CH_2$), 3.33 (m, 16H, NCH_2), 1.04 (t, $^3J = 6.8$ Hz, 24H, CH_3). ^{13}C NMR (CD_2Cl_2, 150 MHz): δ 158.1 and 87.3 ($C=CH_2$), 128.2 (ipso-C of C_5H_4), 110.8 (C3, C4 of C_5H_4), 108.3 (C2, C5 of C_5H_4), 44.4 and 15.6 (NCH_2CH_3). The NMR assignments were secured by GCOSY, GHSQC, and GHMBC 2D NMR experiments.[39]

X-ray Crystal Structure Analysis of 18. Single crystals were obtained from a dichloromethane solution at −20 °C. Formula $C_{15}H_{26}N_2OZr$, $M = 341.60$, colorless crystal 0.65 × 0.40 × 0.10 mm, $a = 9.712(1)$, $b = 13.666(1)$, $c = 14.253(1)$ Å, $\alpha = 69.70(1)$, $\beta = 74.76(1)$, $\gamma = 71.16(1)°$, $V = 1654.7(2)$ Å^3, $\rho_{calc} = 1.371$ g cm^{-3}, $\mu = 6.60$ cm^{-1}, absorption correction via SORTAV ($0.674 \le T \le 0.937$), $Z = 4$, triclinic, space group $P\bar{1}$ (No. 2), $\lambda = 0.71073$ Å, $T = 198$ K, ω and

(37) Firth, A. V.; Stewart, J. C.; Hoskin, A. J. Stephan, D. W. *J. Organomet. Chem.* **1999**, *591*, 185−193. Antiñolo, A., Carrello-Hermosilla, F.; Corrochano, A.; Fernández-Baeza, J.; Lara-Sanchez, A.; Ribeiro, M. R.; Lanfranchi, M.; Otero, A.; Pellinghelli, M. A.; Portela, M. F.; Santos, J. V. *Organometallics* **2000**, *19*, 2837−2843. Nomura, K.; Oya, K.; Komatsu, T.; Imanishi, Y. *Macromolecules* **2000**, *33*, 3187−3189. Zhu, F.; Fang, Y.; Chen, H.; Lin, S. *Macromolecules* **2000**, *33*, 5006−5010. Nomura, K.; Komatsu, T.; Imanishi, Y. *Macromolecules* **2000**, *33*, 8122−8124. Sinnema, P.-J.; Spaniol, T. P.; Okuda, J. *J. Organomet. Chem.* **2000**, *598*, 179−181. Murray, M. C.; Baird, M. C. *J. Polym. Sci., Part A: Polym. Chem.* **2000**, *38*, 3966−3976.

(38) Kempe, P.; Brenner, S.; Arndt, P. *Z. Anorg. Allg. Chem*. **1995**, *621*, 2021−2024. Benzing, E.; Kornicker, W. *Chem. Ber.* **1961**, *94*, 2263−2267.

(39) Braun, S.; Kalinowski, H. O.; Berger, S. *150 and More Basic NMR Experiments*; VCH: Weinheim, 1998; and references therein.

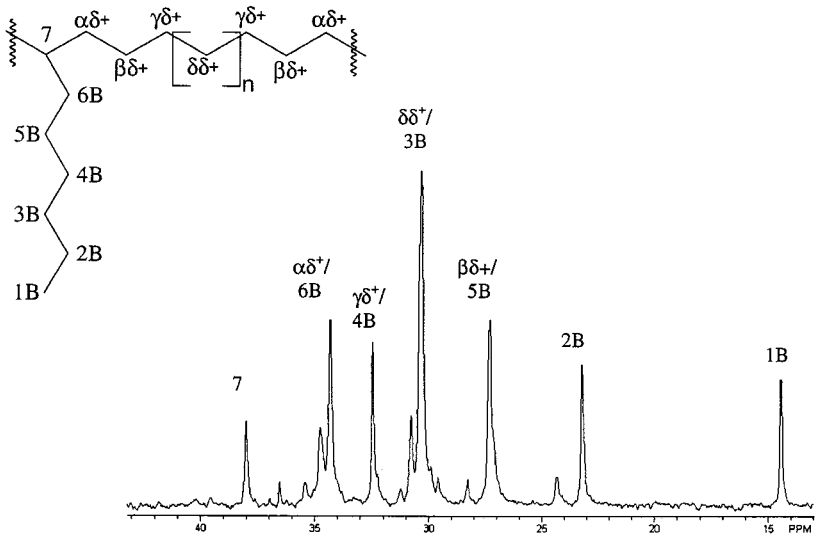

Figure 9. ^{13}C NMR spectrum of the ethene/1-octene copolymer (sample 8 of Table 2) in benzene-d_6.

Chart 4 Catalyst Precursors Used for the Reference Copolymerization Reactions

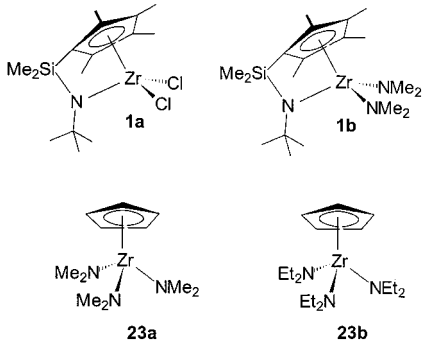

φ scans, 30 411 reflections collected ($\pm h$, $\pm k$, $\pm l$), [(sin θ)/λ] = 0.65 Å^{-1}, 7523 independent (R_{int} = 0.029) and 6829 observed reflections [$I \geq 2\ \sigma(I)$], 351 refined parameters, R = 0.025, wR^2 = 0.062, max residual electron density 0.40 (−0.46) e Å^{-3}, two nearly similar "half molecules" in the asymmetric unit, hydrogens calculated and refined as riding atoms.

Data sets were collected with a Nonius KappaCCD diffractometer, equipped with a rotating anode generator Nonius FR591. Programs used: COLLECT (Nonius, B.V., 1998), data reduction Denzo-SMN (Otwinowski, Z.; Minor, W. *Methods Enzymol.* **1997**, *276*, 307−326.), absorption correction SORTAV (Blessing, R. H. *Acta Crystallogr.* **1995**, *A51*, 33−37; *J. Appl. Crystallogr.* **1997**, *30*, 421−426.), structure solution SHELXS-97 (Sheldrick, G. M. *Acta Crystallogr.* **1990**, *A46*, 467−473.), structure refinement SHELXL-97 (Sheldrick, G. M., Universität Göttingen, 1997), graphics DIAMOND (Brandenburg, K., Universität Bonn, 1997), and SCHAKAL (Keller, E., Universität Freiburg, 1997).

DFT Calculations. Gradient-corrected density functional calculations were carried out, with corrections for exchange and correlation according to Becke[40] and Perdew,[41] respectively (BP 86). Geometries were optimized using the program system TURBOMOLE[42] within the framework of the RI-J approximation.[43] The main group elements were described by a split-valence basis set[44] with one set of polarization functions for the non-H atoms. Zr was treated by a triple-ζ valence basis set[45] plus polarization, in combination with an effective core potential[46] for the description of the innermost 28 electrons.

For the fragment orbital analysis, single-point calculations have been performed with the ADF program package,[47−49] version 2000.02. A triple-ζ basis with one polarization function was employed, and the 1s, 2s, and 2p orbitals of Zr were kept frozen. The geometry was symmetrized according to C_s symmetry, and the Zr−X distance was set to 2.10 Å in all cases.

The same ADF program package and electronic configurations have been used for the DFT calculations of the ethylene insertion reactions. The insertion profiles were calculated by a linear transit search from the free reactants to the final product along a reaction coordinate. The methodology used is similar as the one described by Ziegler et al. for ethylene insertions into metallocene cations and various other Cp-containing Ziegler−Natta catalyst systems.[32] In the calculations, a reaction coordinate R_{CC} defined as the distance between one ethylene terminus and the "active" CH_3 carbon atom has been varied by step simulating the approach and then by the insertion of a molecule of ethylene into the Zr−C bond of both "CpCO"$ZrCH_3^+$ monomer and dimer. Along the linear transit search, the reaction coordinate R_{cc} was kept fixed (values from higher than 4 Å to 1.5 Å) while all other structural parameters were fully optimized. Full transition-state searches were started from geometries corresponding to maxima along the ethylene insertion hypersurfaces.

Polymerization Reactions. A. Ethene Polymerization. The polymerization experiments were carried out in a thermostated 1-L Büchi glass autoclave. The reaction mixtures contained 200 mL of toluene and ca. 20 mL of a 10% MAO solution in toluene. The solution was saturated with ethene at 2 bar for 45 min before the polymerization reactions were started by injection of the group 4 metal catalyst precursors, dissolved in 5 mL of toluene. The reactions were stopped by the addition of 20 mL of a 1:1 mixture of 1 N aqueous HCl in methanol after the pressure was relaxed and the excess ethene was vented. The mixture was stirred for 1 h, then 200 mL of half

(40) Becke, A. D. *Phys. Rev.* **1988**, *A38*, 3098−3100.
(41) Perdew, J. P. *Phys. Rev.* **1986**, *B33*, 8822−8824.
(42) Ahlrichs, R.; Bär, M.; Häser, M.; Horn, H.; Kölmel, C. *Chem. Phys. Lett.* **1989**, *162*, 165−169. Treutler, O.; Ahlrichs, R. *J. Chem. Phys.* **1995**, *102*, 346−354. Ahlrichs, R.; von Arnim, M. In *Methods and Techniques in Computational Chemistry: METECC-95;* Clementi, E., Corongiu, G., Eds.; STEF: Cagliari, 1995; Chapter 13.
(43) Eichkorn, K.; Treutler, O.; Öhm, H.; Häser, M.; Ahlrichs, R. *Chem. Phys. Lett.* **1995**, *242*, 652−670. Eichkorn, K.; Weigand, F.; Treutler, O.; Ahlrichs, R. *Theor. Chem. Acc.* **1997**, *97*, 119−124.
(44) Schäfer, A.; Horn, H.; Ahlrichs, R. *J. Chem. Phys.* **1992**, *97*, 2571−2577.
(45) Schäfer, A.; Huber, C.; Ahlrichs, R. *J. Chem. Phys.* **1994**, *100*, 5829−5835.
(46) Andrae, D.; Häussermann, U.; Dolg, M.; Stoll, H.; Preuss, H. *Theor. Chim. Acta* **1990**, *77*, 123−141.
(47) Baerends, E. J.; Ellis, D. E.; Ros, P. *Chem. Phys.* **1973**, *2*, 41−51.
(48) te Velde, G.; Baerends, E. J. *J. Comput. Phys.* **1992**, *99*, 84−98.
(49) Fonseca Guerra, C.; Snijders, J. G.; te Velde, G.; Baerends, E. J. *Theor. Chem. Acc.* **1998**, *99*, 391−403.

concentrated aqueous HCl was added. The polyethylene was collected by filtration, washed with toluene, and diluted in aqueous HCl, water, and acetone and then was dried in vacuo (for further details see Table 2).

B. Ethene/1-Octene Copolymerization. The copolymerization reactions were carried out in a 1-L Büchi glass autoclave using a mixture of 50 mL of 1-octene, 30 mL of toluene, and 20 mL of a 10% MAO solution in toluene. Saturation with ethene was achieved at 1 bar for 45 min at the reaction temperature of 90 °C. The copolymerization reaction was started by the injection of the solution of the group 4 metal catalyst precursor dissolved in 5 mL of toluene. The reaction was quenched with 20 mL of 1 N aqueous HCl in methanol (1:1), stirred for 1 h to remove excess ethene. Then 200 mL of half concentrated aqueous HCl was added. Workup was usually carried out by separation of the organic phase, extraction of the aqueous phase with toluene (2 x), washing of the combined organic solutions with dilute HCl, then water. Solvent was then removed in vacuo to yield the ethene/1-octene copolymers, that were mostly obtained as viscous oils. Characterization by ^{1}H decoupled ^{13}C NMR (benzene-d_6, 50 MHz, polymer sample nr. 8, see Table 2 and Figure 9):[35] δ 38.0 (C7), 34.3 ($C_{\alpha\delta+}$, C_{6B}), 32.4 ($C_{\gamma\delta+}$, C_{4B}), 30.3 ($C_{\delta\delta+}$, C_{3B}), 27.3 ($C_{\beta\delta+}$, C_{5B}), 23.1 (C_{2B}), 14.4 (C_{1B}). The ethene/1-octene ratio of the copolymer was determined by integrating the ($C_{\delta\delta+}$, C_{3B}), ($C_{\alpha\delta+}$, C_{6B}), and ($C_{\beta\delta+}$, C_{5B}) signals. The ethene/1-octene ratio was calculated as $2 + (3a - 1)/2$ with $a = I(C_{\delta\delta+}, C_{3B})/I(C_{\alpha\delta+}, C_{6B}) = I(C_{\delta\delta+}, C_{3B})/I(C_{\beta\delta+}, C_{5B})$.

Acknowledgment. Financial support by the Fonds der Chemischen Industrie, the Deutsche Forschungsgemeinschaft, and COST (program D12/0016/98, contract no. CJJ.004) is gratefully acknowledged.

Supporting Information Available: Details of the X-ray crystal structure analyses of the compounds **11** and **18**; ^{13}C NMR spectra of additional ethene/1-octene copolymer samples; geometries and bond energies for all DFT optimized structures; further schemes and figure concerning the calculated ethylene insertion profiles (PDF). This material is available free of charge via the Internet at http://pubs.acs.org.

JA010943B